Heliyon 10 (2024) e34036

Contents lists available at ScienceDirect

Heliyon

journal homepage: www.cell.com/heliyon

Research article

Binding of green tea epigallocatechin gallate to the arginine kinase active site from the brown recluse spider (*Loxosceles laeta*): A potential synergist to chemical pesticides

Elena N. Moreno-Cordova [a,**,1], Andres Alvarez-Armenta [b,1], Karina D. Garcia-Orozco [a], Aldo A. Arvizu-Flores [c], Maria A. Islas-Osuna [d], Ramon E. Robles-Zepeda [c], Alonso A. Lopez-Zavala [c], Aldana Laino [e], Rogerio R. Sotelo-Mundo [a,*]

[a] *Laboratorio de Estructura Biomolecular, Centro de Investigación en Alimentación y Desarrollo, A. C., Hermosillo, Sonora, Mexico*
[b] *Departamento de Microbiología Molecular, Instituto de Biotecnología, Universidad Nacional Autónoma de México, Avenida Universidad 2001, Cuernavaca, Morelos, 62210, Mexico*
[c] *Departamento de Ciencias Químico Biológicas, Universidad de Sonora, Hermosillo, Sonora, Mexico*
[d] *Laboratorio de Biología Molecular de Plantas, Centro de Investigación en Alimentación y Desarrollo, A. C., Hermosillo, Sonora, Mexico*
[e] *Instituto de Investigaciones Bioquímicas de La Plata "Prof. Dr. Rodolfo R. Brenner" (INIBIOLP), Centro Científico Tecnológico – La Plata CONICET- Univerdad Nacional de La Plata, La Plata, Argentina*

ARTICLE INFO

Keywords:
Spider
Loxosceles laeta
Arginine kinase
Green tea
Epigallocatechin gallate
Molecular dynamics
Docking

ABSTRACT

Loxosceles spp. spiders can cause serious public health issues. Chemical control is commonly used, leading to health and environmental problems. Identifying molecular targets and using them with natural compounds can help develop safer and eco-friendlier biopesticides. We studied the kinetics and predicted structural characteristics of arginine kinase (EC 2.7.3.3) from *Loxosceles laeta* (*Ll*AK), a key enzyme in the energy metabolism of these organisms. Additionally, we explored (−)-epigallocatechin gallate (EGCG), a green tea flavonoid, as a potential lead compound for the *Ll*AK active site through fluorescence and *in silico* analysis, such as molecular docking and molecular dynamics (MD) simulation and MM/PBSA analyses. The results indicate that *Ll*AK is a highly efficient enzyme (K_m^{Arg} 0.14 mM, K_m^{ATP} 0.98 mM, k_{cat} 93 s^{-1}, k_{cat}/K_m^{Arg} 630 s^{-1} mM^{-1}, k_{cat}/K_m^{ATP} 94 s^{-1} mM^{-1}), which correlates with its structure similarity to others AKs (such as *Litopenaeus vannamei*, *Polybetes pythagoricus*, and *Rhipicephalus sanguineus*) and might be related to its important function in the spider's energetic metabolism. Furthermore, the MD and MM/PBSA analysis suggests that EGCG interacted with *Ll*AK, specifically at ATP/ADP binding site (RMSD <1 nm) and its interaction is energetically favored for its binding stability (−40 to −15 kcal/mol). Moreover, these results are supported by fluorescence quenching analysis (K_d 58.3 μM and K_a 1.71×10^4 M^{-1}). In this context, *Ll*AK is a promising target for the chemical control of *L. laeta*, and EGCG could be used in combination with conventional pesticides to manage the population of *Loxosceles* species in urban areas.

* Corresponding author. Rogerio Sotelo-Mundo, Ph.D. Carretera Gustavo Enrique Astiazarán Rosas Núm. 46, Ejido a la Victoria, Hermosillo 83304, Sonora, Mexico.
** Corresponding author. Elena N. Moreno-Córdova, Ph.D. Carretera Gustavo Enrique Astiazarán Rosas Núm. 46, Ejido a la Victoria, Hermosillo, 83304, Sonora, Mexico.
E-mail addresses: noheli.moreno@ciad.mx (E.N. Moreno-Cordova), rrs@ciad.mx (R.R. Sotelo-Mundo).
[1] Both persons are the first authors.

https://doi.org/10.1016/j.heliyon.2024.e34036
Received 12 March 2024; Received in revised form 30 June 2024; Accepted 2 July 2024
Available online 3 July 2024

1. Introduction

Loxosceles is a genus of spiders, commonly known as brown recluse spiders, fiddle-back or violin spiders, which are identified by the distinctive violin-shaped mark on their cephalothorax [1–3]. These spiders are well-adapted to urban environments and are responsible for numerous medical cases worldwide. With over 140 species described to date, most are found in the American continent, west India, and Africa, but some species have also been reported in Mediterranean Europe and China [4]. The venom of *Loxosceles* spiders is a complex mixture of toxins, including phospholipases D, astacin-type metalloproteases, and low molecular weight peptides (knottins or inhibitor cystine knot peptides) [5,6]. A bite from a *Loxosceles* spider can cause loxoscelism in 75–80 % of cases, which is characterized by dermo necrosis near the bite site [2,6,7]. 20–25 % of bites can cause systemic toxicity, especially in children, teenagers, and elderly adults, which can result in hemolysis, hemolytic anemia, thrombocytopenia, and acute renal failure [6,8,9].

L. laeta is predominantly distributed in the American continent, promoting the cutaneous-hemolytic form of loxoscelism as a public health problem [6,9–11]. However, epidemiological data on this disease is scarce and it may be underestimated due to the lack of methods to accurately diagnose it [12]. Most clinical diagnoses are still based on a spider bite history or the appearance of necrotic skin lesions [13,14]. The increasing reports of loxoscelism result from the ecological imbalance caused by the extinction of predators, climate change, and pest management practices, resulting in the spider's adaptation to urban environments [14,15]. In this sense, minimizing human-spider contact is key to preventing spider bite accidents, and effective control methods are essential for successful prevention [2].

Pesticides like lindane and chlordane, previously used against *Loxosceles* spiders, are banned due to their carcinogenic effects, environmental pollution, and bioaccumulation [16]. Likewise, the pyrethroid lambda-cyhalothrin effectively reduced the *L. intermedia* population, however, it requires a higher concentration than permitted and may lead to resistance [17]. Therefore, it is crucial to develop new control strategies to reduce infestations of *Loxosceles* spiders safely. For example, Ewing et al. [18] employed plant-derived essential oils to manage *L. reclusa*, significantly decreasing their population. In this sense, exploring natural compounds represents a promising approach for further research.

Phosphagens are energy-storing compounds that are an immediate access reserve of high-energy phosphates when adenosine triphosphate (ATP) turnover is needed [19]. To keep energy levels stable, specific phosphagen molecules are required to transfer phosphate to adenosine diphosphate (ADP) and then transfer it back when enough ATP is available [19]. Invertebrates use phosphoarginine as a phosphagen; this is synthesized by arginine phosphorylation (PO_4^-), catalyzed by arginine kinase (AK) (EC 2.7.3.3) [19,20]. AK is vital for the survival of certain parasites under stress conditions where ATP demand is high and is present in high energy-demanding tissues of insects, confirming its physiological and biochemical functions [21,22]. Spiders need ATP for quick movements during hunting, wandering, or jumping, which is limited by phosphagen depletion [23,24]. Inhibiting AK increases insect susceptibility to deltamethrin, suggesting its role in detoxifying pesticides [25]. This highlights the potential of AK as a promising target for developing innovative techniques to manage spiders. Nevertheless, the kinetic characterization of *L. laeta* AK (*Ll*AK) and its interaction with natural compounds have not been described.

Biopesticides are natural substances that can prevent or reduce pest attacks, showing advantages like eco-friendliness, low toxicity, biodegradability, and selectivity [26]. They can be sourced from plants; among these, phenolic compounds are secondary metabolites with a wide range of biological and health-promoting activities. (−)-Epigallocatechin-3-gallate (EGCG) is the most abundant polyphenol in green tea (*Camellia sinensis*), known for its exceptional broad-spectrum activities as antioxidant, anti-inflammatory, anticancer, anti-microbial, immunomodulatory, and insecticidal [27–29]. Flavonoids exhibit great potential as biopesticides and complement to traditional pesticides against various global pests relevant to food crops [29–31]. In-vivo studies have demonstrated the efficacy of EGCG in altering the activities of detoxification enzymes and inhibiting the development and survival of *Aphis gossypii* [32]. This suggests that EGCG could be used to develop innovative biopesticides because this flavonoid has biodegradable and low-toxicity properties. Similar compounds such as catechin, quercetin, luteolin, and kaempferol have shown in-vivo insecticidal activity in other organisms [29]. Moreover, phenolic compounds like rutin, resveratrol and delphinidin can inhibit AK activity from insects and parasites [33–36], suggesting their potential for innovative biopesticide development.

In this context, molecular dynamic (MD) simulation is a powerful tool for predicting the efficacy of interaction between natural compounds, particularly those found in black tea, and viral molecular targets [37,38]. Moreover, recent applications of MD simulations have led to the development of innovative management strategies [39]. Implementing this bioinformatic tool can contribute to the design of new biopesticides using *Ll*AK as a molecular target and EGCG as a potential lead compound, contributing to the control of the *L. laeta* spider population.

Therefore, this study examined the structure and kinetics of *Ll*AK. It also evaluated the potential of (−)-epigallocatechin gallate (EGCG) as a lead compound for the *Ll*AK's active site through molecular docking and dynamic simulation. The research could provide valuable insights for developing safer, eco-friendly, and more effective biopesticides for managing spider populations, particularly in urban areas with dangerous *Loxosceles* spiders.

2. Materials & methods

2.1. Arginine kinase expression

The arginine kinase from *L. laeta* (*Ll*AK) construct was assembled using a synthetic DNA gene fragment (gBlocks™ Gene Fragments, Integrated DNA Technologies). The gene fragment was designed to contain the full-length *Ll*AK coding sequence (GenBank

EY188599.1) plus a 6x-His tag at the N-terminal, flanked by restriction sites for *Nde* I and *BamH* I enzymes for directional cloning. First, *Ll*AK gene fragment was cloned into pJET1.2/blunt® vector (1:3 vector-insert molar ratio) using the PCR CloneJET® kit (ThermoFisher Scientific). The recombinant plasmid pJET1.2/blunt-*Ll*AK and the protein expression vector pET11-a(+) (Novagen) were digested using *Nde* I and *BamH* I restriction enzymes (New England BioLabs). Then, *Ll*AK insert was ligated into the pET11-a(+) vector for directional subcloning at 1:3 vector-insert molar ratio. Ligation was carried out at 4 °C overnight using T4 DNA ligase in the reaction buffer supplemented with ATP. The ligation reaction transformed *E. coli* TOP10 competent cells by heat shock. The subcloning process was verified by colony PCR from positive clones and Sanger sequencing. Finally, recombinant plasmid DNA pET11-a(+)-*Ll*AK was isolated and purified using Wizard® Plus SV Minipreps DNA Purification System (Promega).

The construct pET11-a(+)-*Ll*AK was used to transform *E. coli* BL21 Gold (DE3) competent expression cells by heat shock, and the cells were incubated in SOC medium at 37 °C/90 min with shaking at 225 rpm. Subsequently, the bacterial suspension was cultured in Luria Broth (LB) plates with ampicillin (100 μg mL^{-1}) and then incubated at 37 °C overnight. A single-isolated colony of the transformation reaction was inoculated in 5 mL of LB medium, supplemented with ampicillin (100 μg mL^{-1}), and grown at 37 °C overnight with shaking at 225 rpm. This culture was used as the starting bacterial inoculum for 1 L of LB broth supplemented with ampicillin (100 μg mL^{-1}) and grown at 37 °C and 225 rpm until cell density reached 0.6 at OD_{600nm}. *Ll*AK overexpression was induced by adding 0.2 mM IPTG (isopropyl-β-D-thiogalactopyranoside), and the culture was kept growing at 25 °C/18 h and 220 rpm. Bacterial cells were harvested by centrifugation at 7000×*g*/20 min (at 4 °C), and the cell pellet was stored at −80 °C until use.

2.2. Purification of recombinant *Ll*AK

The pellet was suspended in lysis buffer (20 mM Tris-HCl, 500 mM NaCl, 0.5 mM PMSF, 5 mM benzamidine, 1 mM DTT, pH 7.0) at 1:4 (w/v) and lysed by sonication at 40 % amplitude during 10 s for 6 times with 60 s rest intervals, keeping the sample on ice. The lysate was clarified by centrifugation at 10,000×*g*/20 min at 4 °C and *Ll*AK was purified by IMAC using a 5 mL Ni-NTA HisTrap™ HP column (Cytiva Life Sciences) on an ÄKTA Prime Plus chromatographer (GE Life Sciences). Briefly, the column was equilibrated with binding buffer (20 mM Tris-HCl, 500 mM NaCl, pH 7.5) and loaded with the crude extract containing *Ll*AK. Next, recombinant His-tagged *Ll*AK was eluted using a 0–60 % linear gradient of imidazole with elution buffer (20 mM Tris-HCl, 500 mM NaCl, 500 mM imidazole, pH 7.5) at a flow rate of 1 mL/min. The presence of protein was monitored at 280 nm. Eluted fractions were collected and analyzed by reducing SDS-PAGE.

Fractions containing a band with a molecular weight of 40 kDa were pooled and dialyzed against 50 mM Tris-HCl, 150 mM NaCl (pH 7.5) buffer using a 6–8 kDa cut-off membrane (Spectra/Por® Dialysis membrane, Spectrum® Laboratories) at 4 °C. Then, the protein was concentrated by centrifugation at 6000 rpm/4 °C using an Amicon® Ultra-15 (30 kDa cut-off) membrane (Merk Millipore) and subjected to SEC as a second purification step using a Superdex® 75 10/300 GL gel filtration column on an ÄKTA Pure chromatograph (Cytiva Life Sciences). *Ll*AK was eluted using Tris-HCl buffer (50 mM, 150 mM NaCl, pH 7.5) at a 0.5 mL/min flow rate. The purity of *Ll*AK was determined by electrophoretic analysis of elution peaks. Protein concentration was estimated by $A_{280\ nm}$ using $\varepsilon =$ 25, 900 M^{-1} cm^{-1} calculated from *Ll*AK amino acid sequence in ProtParam tool and by the bicinchoninic acid method using the Micro BCA™ Protein Assay kit (Thermo Scientific) at 595 nm on a microplate reader using BSA as the protein standard.

2.3. Kinetic characterization of *Ll*AK

The enzymatic activity of *Ll*AK was determined using the coupled enzyme assay described by Ref. [40], with some modifications [24,41]. This method uses a system of three coupled enzymatic reactions: AK phosphorylates L-arginine using a phosphate group from ATP, producing L-arginine and ADP. Then, pyruvate kinase phosphorylates ADP again using phosphoenol pyruvate, forming pyruvate and ATP. Finally, lactate dehydrogenase reduces pyruvate to lactate by oxidizing NADH to NAD^+. AK activity was calculated from the consumption of NADH, spectrophotometrically measured as a decrease in absorbance at 340 nm during 4 min at 30 °C in a Cary-50 (Varian) UV spectrophotometer. The *Ll*AK activity was calculated using the molar extinction coefficient of β-NADH ($\varepsilon = 6.22$ mM^{-1} cm^{-1}) at 340 nm [40]. One unit of arginine kinase activity is defined as the amount of enzyme that produces 1.0 μmol of phospho--L-arginine per minute at pH 8.6 and 30 °C [42].

The reaction contained final concentrations of 178 mM glycine buffer pH 8.6, 0.33 mM 2-mercaptoethanol, 133 mM potassium chloride, 13 mM magnesium sulfate, 20 mM phosphoenol pyruvate, 6.7 mM ATP, 0.13 mM β-NADH, 2 U of pyruvate kinase, 3 U of lactate dehydrogenase, 17 mM L-arginine, and 0.44 μM of *Ll*AK. The kinetic constants for both substrates were determined by varying one substrate concentration while maintaining a fixed saturating concentration of the other. The final L-arginine concentrations ranged from 0.078 mM to 10 mM, whereas ATP varied from 0.0523 mM to 6.7 mM. Control reactions without *Ll*AK enzyme, arginine, or ATP were performed for background correction. The kinetic parameters K_m and V_{max} were estimated by fitting the initial reaction rates to the Michaelis-Menten equation model (Eq. (1)) by non-linear regression analysis. Moreover, the catalytic constant (k_{cat}) was determined using Equation (2). All experimental data were analyzed in GraphPad Prism v9.5.1 (GraphPad Software, San Diego, California, USA).

$$V_0 = \frac{V_{max}\, S}{K_m + S} \tag{1}$$

$$k_{cat} = \frac{V_{max}}{[E]} \tag{2}$$

Where V_0 is the initial velocity, V_{max} is the maximal velocity, K_m is the Michaelis-Menten constant, S is the concentration of variable substrate, [E] is the enzyme concentration in the reaction and k_{cat} is the enzyme's catalytic constant.

2.4. Bioinformatic analysis of conserved domains and structural features in LlAK

The amino acid sequence of *Ll*AK was deduced from an EST cDNA library of *L. laeta* venomous gland, previously reported by Ref. [43] (BioSample: SAMN00154551) and *Ll*AK full-length mRNA of 1254 bp (GenBank EY188599). Physicochemical parameters of *Ll*AK were computed using the ProtParam tool (https://web.expasy.org/protparam/) [44]. Multiple sequences alignment of arginine kinases was performed using the T-Coffee server (https://tcoffee.crg.eu/) [45] and analyzed using the Mview tool from the EMBL-EBI server (https://www.ebi.ac.uk/Tools/msa/mview/) [46]. Conserved domains of *Ll*AK amino acid sequences were identified using the NCBI Conserved Domain Database (https://www.ncbi.nlm.nih.gov/cdd/) [47], and the protein's subcellular location was predicted using the SignalP v6.0 server (https://services.healthtech.dtu.dk/services/SignalP-6.0/) [48].

In the case of the *Ll*AK structure (in the open conformation) was predicted *de novo* by artificial intelligence (AI) technology using ColabFold v1.5.2 (AlphaFold2 using Mmseqs2 software) (https://github.com/sokrypton/ColabFold) [49]. Default parameters were no template information, 24 recycles, and AMBER refinement. In addition, a molecular model in the closed-active conformation was obtained by homology to the AK from *Litopenaeus vannamei* in complex with arginine and ADP (PDB: 4BG4). The homology model was constructed using Molecular Operating Environment Software (MOE) v2022.02 (Chemical Computing Group ULC, Montreal, Canada), including the ligands during the minimization step of the final model under the CHARMM27 forcefield.

2.5. LlAK-EGCG interactions by molecular docking

Molecular docking was performed to predict *Ll*AK and EGCG interactions. The preparation of the receptor (*Ll*AK model in closed-active conformation), the ligand (EGCG, PubChem CID: 65064), and the cavity selection for molecular docking were performed in MOE. Partial charges of EGCG were assigned using the PEOE method [50]. The cleft comprising the arginine and ATP/ADP binding sites in *Ll*AK model was set as the docking site, where five independent docking runs were performed under the MMFF94x forcefield. For the EGCG placement at the docking site, we used the alpha-triangle method with the London ΔG scoring function to sample the best 30 top-scoring poses from at least 80,000 iterations. A post-placement refinement step was done to optimize further and collect only the best five top-scoring predicted poses with a rigid receptor methodology and the affinity ΔG-scoring function. Finally, the score values, ligand fitness, and pose redundancy were analyzed. All analyses and figures were prepared in MOE v2022.02 (Chemical Computing Group ULC, Montreal, Canada).

2.6. Stability of ECCG interactions by molecular dynamics and molecular mechanic Poisson–Boltzmann surface area

Molecular dynamics (MD) simulations were employed to understand the stability of substrates (ATP and arginine as controls) and *Ll*AK-EGCG complex and to correlate its effect to *Ll*AK inhibition. For this objective, the topologies of docked *Ll*AK-EGCG's complex obtained by MOE were prepared using the CHARMM-GUI webserver (https://www.charmm-gui.org/) and further parameterized using the CHARMM36 force field. The simulation system was solvated using the TIP3 water model and neutralized with three Na^+ ions. Following, the system was energy minimized using the steepest descending algorithm (5000 descending steps) and equilibrated at 303.15 K using 200 ps NVT/NPT ensembles before production molecular simulation runs (100 ns) were performed by duplicate. Parriello-Rahman pressure and Nose-Hoover temperature controller systems were employed throughout the equilibration to maintain a constant pressure of 1 bar and 303.15 K. Moreover, the particle mesh Ewald (PME) method was considered for calculating long-range electrostatic interactions. The Verlet scheme with a cutoff value of 1 nm was utilized to calculate short-range van der Waals interactions. At the same time, Linear Constraint Algorithm (LINCS) was employed to constrain all the covalent bond lengths, including the hydrogen bond. MD simulations were carried out using GROMACS (version 2022.4) software, and trajectories were conducted to obtain binding parameters of the *Ll*AK-EGCG interactions, such as ECCG to *Ll*AK root mean square deviation (RMSD) of backbone C-α atoms (gmx rms script) and the number of hydrogen bonds (gmx hbond script) between *Ll*AK and EGCG. Moreover, the Molecular Mechanic Poisson–Boltzmann Surface Area (MM/PBSA) method was employed to analyze the interactions of *Ll*AK-EGCG complexes using the gmx_MMPBSA program [51]. The complete MD simulation trajectory (100 ns) was evaluated to compute diverse elements of binding free energy and decomposition analysis by residue (within 4 Å) during *Ll*AK–EGCG interaction.

2.7. Fluorescence quenching of LlAK by EGCG

Quenching of intrinsic tryptophan fluorescence was performed to investigate interactions between *Ll*AK and EGCG. Fluorometric titrations were carried out in a reaction mixture in sodium phosphate buffer (50 mM, pH 7.0) at 25 °C with 1 μM *Ll*AK and increasing EGCG concentrations (0 μM–130 μM, dissolved in ultrapure water). Steady-state fluorescence of *Ll*AK was monitored in the absence and EGCG presence. The excitation wavelength (λ_{ex}) was 295 nm and its emission spectra (λ_{em}) were collected in a QM-2003 spectrofluorometer (Photon Technology International, Edison, NJ, USA) at the range of 300–500 nm and excitation and emission monochromators were manually set at 5 nm and 10 nm slit widths, respectively. For graphical representation, fluorescence emission spectra were smoothed using the Savitzky-Golay filtering method (2nd order smoothing at 9 neighboring data points) and all analyses were carried out in GraphPad Prism v9.5.1 (GraphPad Software, San Diego, California, USA). The dissociation constant (K_d) of EGCG

was estimated from the fluorescence intensity change in *Ll*AK's at maximum λ_{em}^{325nm} *versus* EGCG concentration by non-linear fit analysis (one-site binding). In all cases, the data were corrected from inner filter effects (Eq. (3)), and the linear Stern-Volmer equation (Eq. 4) was used to obtain the quenching constant (K_{sv}) [52].

$$F_{corr} = F_{obs} \text{ anti log}\left(\frac{OD_{ex} + OD_{em}}{2}\right) \tag{3}$$

Where: F_{corr} is the fluorescence corrected from inner filter effects, F_{obs} is the observed fluorescence emission, and OD_{ex} and OD_{em} are the absorbance values at the excitation and emission wavelengths, respectively.

$$\frac{F_0}{F} = 1 + K_{SV}[Q] \tag{4}$$

Where: F_0 and F are the *Ll*AK fluorescence intensities in absence and EGCG presence, respectively. [Q] is the EGCG concentration and K_{sv}.

The modified Stern-Volmer equation [53] (Eq. (5)) was applied to proteins with two tryptophan fractions, one accessible and the other inaccessible to the quencher.

$$\frac{F_0}{\Delta F} = \frac{1}{f_a K_q} \times \frac{1}{[Q]} + \frac{1}{f_a} \tag{5}$$

Where: ΔF is equal to $F_0 - F$, f_a (intercept) is the fraction of fluorophore accessible to EGCG, K_q (slope of the $F_0/\Delta F$ *versus* 1/[Q] plot) is the modified Stern-Volmer quenching constant, analogous to the binding association constant.

Finally, fluorescence measurements are useful for obtaining quantitative information about protein-ligand binding. A double logarithmic equation can be applied in proteins with more than one possible binding site (Eq. (6)).

$$\text{Log}\left(\frac{F_0 - F}{F}\right) = \log K_a + n \log [Q] \tag{6}$$

Where: K_a is the binding constant for the macromolecule-quencher interaction and n is the number of binding sites per macromolecule. Both can be determined from the intercept and the slope of the double logarithm regression curve.

3. Results

3.1. Kinetic characterization of *Ll*AK

*Ll*AK was produced and purified by His-tag as a recombinant protein identified by SDS-PAGE at 42 kDa (Fig. S1) with a yield of ~27 mg/L of *E. coli* culture. The *Ll*AK-specific activity was 1.1 U/mg, demonstrating its active form. The kinetic parameters (Table 1) for L-arginine (Fig. 1A) and ATP (Fig. 1B) substrates were obtained from the non-linear fitting of initial velocities to the Michaelis-Menten equation (Fig. 1). Arginine showed the highest affinity for *Ll*AK active site, reflected in the lowest K_m value (0.14 mM) compared to those reported for other AKs from different invertebrate species [24,54,55]. Conversely, ATP showed the highest K_m and, hence, the lowest affinity to *Ll*AK. The high catalytic efficiency of *Ll*AK is evidenced in the turnover number (k_{cat} 93 s^{-1}) and the k_{cat}/K_m ratio. The k_{cat} value describes how many substrate molecules are transformed into the L-arginine product per second by a single *Ll*AK monomer. In contrast, the k_{cat}/K_m ratio relates to the enzyme's catalytic efficiency concerning each substrate. In this sense, *Ll*AK exhibited higher catalytic efficiency for arginine (630 s^{-1} mM^{-1}) than for ATP (94 s^{-1} mM^{-1}).

3.2. Conserved domains in *Ll*AK

The AK sequences are conserved in the invertebrate phylum, and the subcellular location of *Ll*AK was predicted to be a cytosolic phosphagen kinase [20]. *Ll*AK showed high sequence identity with AKs from other arthropod species, such as *Polybetes pythagoricus*

Table 1
Kinetic parameters of *Ll*AK for the arginine and ATP substrates, and comparison with arginine kinases from other invertebrate species.

Species	V_{max} (μmol min^{-1})	K_m^{Arg} (mM)	K_m^{ATP} (mM)	k_{cat} (s^{-1})	k_{cat}/K_m^{Arg} (s^{-1} mM^{-1})	k_{cat}/K_m^{ATP} (s^{-1} mM^{-1})	References
Brown recluse spider (*L. laeta*)	21 ± 0.002	0.1470 ± 0.07	0.98 ± 0.42	93 ± 10	630.6	94.05	This work
Giant crab spider (*P. pythagoricus*)	27.8	1.7	NR	75	44.4	NR	[25]
Brown tick (*R. sanguineus*)	26.1	0.27 ± 0.08	0.31 ± 0.12	142 ± 0.21	523.2	458.1	[50]
American crockoach (*P. americana*)	21.7	0.49	0.14	1.3	2.7	9.3	[51]

NR: Not reported.

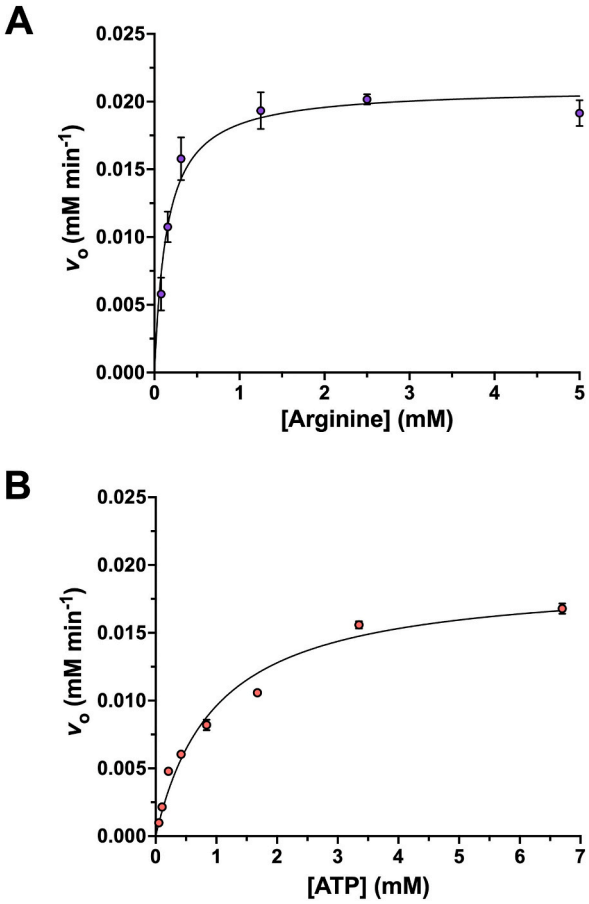

Fig. 1. Michaelis-Menten plots of *Ll*AK kinetics with L-arginine and ATP substrates. A) *Ll*AK kinetics with L-arginine (0.078 mM–5 mM) at fixed ATP concentration (6.7 mM). B) *Ll*AK kinetics with ATP (0.0523 mM–6.7 mM) at fixed L-arginine concentration (17 mM). Data are presented as the mean ± standard deviation.

(84 %), *Limulus polyphemus* (82 %), *Rhipicephalus sanguineus* (79 %), *Lycosa tarantula* (77 %), *L. vannamei* (76 %), *Periplaneta americana* (73 %), and *Latrodectus hesperus* (70 %), but low similarity (44 %) with *Homo sapiens* creatine kinase (Fig. S2). The analysis indicated that *Ll*AK has a highly conserved arginine kinase-like domain from Lys^{9} to Ala^{356} (phosphagen kinases superfamily: ATP-guanidino phosphotransferase, cl02823, Pfam 00217). This large domain contains the well-conserved active site residues (Arg^{126}, Glu^{225}, Arg^{229}, Cys^{271}, Thr^{273}, Arg^{280}, Arg^{309}, and Glu^{314}), the arginine binding site (Ser^{63}, Gly^{64}, Val^{65}, Gly^{66}, Ile^{67}, Tyr^{68}, Phe^{194}, Glu^{225}, Cys^{271}, Thr^{273}, Asn^{274}, Glu^{314}, and His^{315}), the ATP/ADP binding site (Ser^{122}, Arg^{124}, Arg^{126}, His^{185}, Trp^{221}, Arg^{229}), and the two flexible loops Ser^{63}-Tyr^{68} and Leu^{306}-Asn^{327} involved in substrate specificity [56–58].

The open (apo-) and closed (holo-enzyme) *Ll*AK molecular models (Fig. 2) show the characteristic folding of phosphagen kinases, which consists of a small (residues 1–111) N-terminal domain formed by α-helices and a large (residues 112–357) C-terminal domain formed by eight antiparallel β-sheets flanked by seven α-helices, comprising an α-β fold known as the guanidino kinase domain [56]. Moreover, the active site cleft bridges the two domains, where the L-arginine/phospho-L-arginine binding site is located between the N- and C-terminal domains of the enzyme, while the ATP/ADP binding site localizes at the large C-terminal domain where most of the catalytic residues are found [56,58,59] (Fig. 2B). Superposition of the open-inactive and closed-active predicted structures of *Ll*AK show significant differences in both protein conformations (RMSD = 1.57 Å) (Fig. 2A). These are mainly in the backbone structures that shape the active site and two flexible loops involved in substrate clamping and specificity (one located in the N-terminal domain, and other in the C-terminal).

3.3. Prediction of interactions between LlAK and EGCG by molecular docking

Molecular docking analysis was performed at the predicted *Ll*AK active site cleft, comprising both substrate binding sites. Docking calculations for arginine and ADP binding to the *Ll*AK active site were carried out as a control to reproduce and compare substrate binding modes. Moreover, a thorough examination of the *Ll*AK model revealed that the active site cleft was the only potential EGCG binding site, as no other pocket was identified.

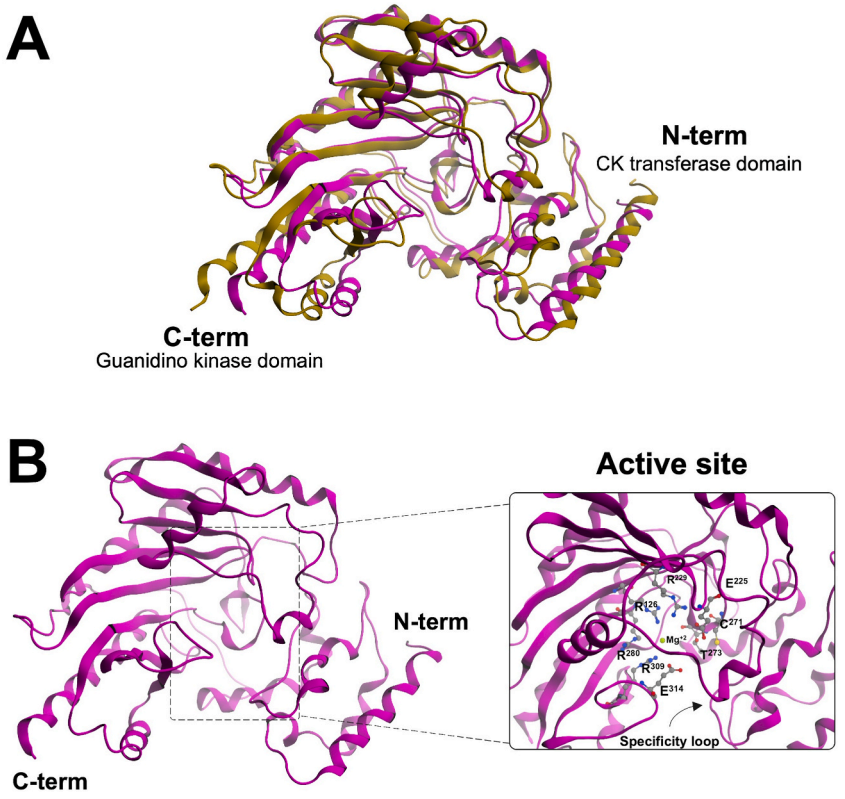

Fig. 2. Molecular model of *Ll*AK tridimensional structure. A) *de novo* prediction of the *Ll*AK tridimensional structure (open conformation, yellow), superposition of open and closed conformations. B) Template-based (homology) prediction of the *Ll*AK tridimensional structure (closed conformation, magenta). Conserved active site residues and structural motifs and signatures are highlighted.

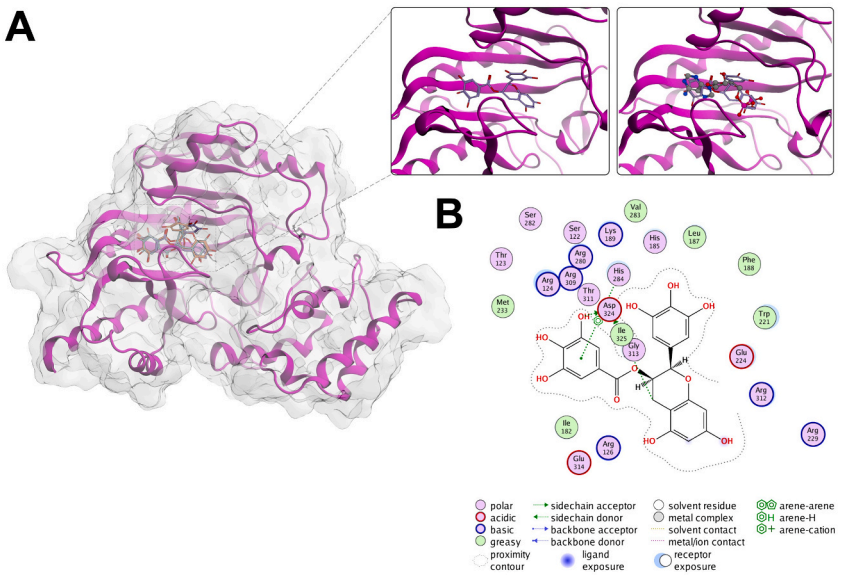

Fig. 3. Molecular docking of the interaction between *Ll*AK and EGCG at the ATP/ADP binding site. A) Surface map and ribbon representation of EGCG binding at the ATP/ADP pocket and superposition of ADP and EGCG structures. B) Lig-plot diagram of EGCG interactions at the ATP/ADP pocket.

The molecular docking between *Ll*AK and EGCG results indicated that EGCG can bind at both substrate-binding sites, although showing different predicted affinities (Figs. 3 and 4). The best-ranked EGCG poses were converged at the ATP/ADP binding site with an average binding score of – 9.43 kcal/mol, which resulted better than the calculated ADP free binding energy (from – 8.3 to −7 kcal/mol) (Fig. 3A). Furthermore, other EGCG poses were predicted to interact at the arginine binding site with a mean binding score of – 7.7 kcal/mol, comparable to the arginine free binding energy (from – 8.0 to −5.0 kcal/mol) (Fig. 4A). Docked EGCG to ATP/ADP binding site revealed hydrogen bonds and pi (arene-arene and arene-hydrogen) molecular interactions with Arg^{324}, His^{284}, Ile^{325} and Gly^{313}, as well as in proximity with essential residues for ATP/ADP interaction at this site, including Arg^{124}, Arg^{126}, His^{185}, and Trp^{221} (Fig. 3B). On the other hand, docking predictions of EGCG to arginine binding site showed hydrogen bonds, pi (arene-hydrogen), and backbone acceptor type interactions with Arg^{280}, Glu^{224}, Glu^{225}, Glu^{314}, Cys^{271}, Val^{65}, and Ile^{67}, identified as essential for AK catalytic activity (Fig. 4B). Other residues in proximity with EGCG that are important for arginine binding and specificity loop were also identified (Ser^{63}, Gly^{64}, Gly^{66}, Tyr^{68}, Phe^{194}, Asn^{274}) (Fig. 4B).

3.4. *Interaction stability between LlAK and EGCG by molecular dynamic simulations*

The MD simulations are used to evaluate and characterize the interaction stability of the protein-ligand complex. Since *Ll*AK possesses two substrate-binding sites, separate MD simulations were conducted for the *Ll*AK-EGCG complexes at each binding site, compared with its substrates. In particular, ATP-binding site MD simulations revealed that the root mean square deviation (RMSD) (Fig. 5A) between *Ll*AK and EGCG exhibited oscillations of <1 nm over time (100 ns), indicating a minimal EGCG displacement from its site. In addition, the hydrogen bond plot (Figs. S3 and S4) shows that EGCG-*Ll*AK interaction is promoted by hydrogen bonds. Its reduction observed at 30–40 ns of simulation time suggests the formation of other interactions, such as hydrophobic bonds were also correlated with the reduction of solvent accessible surface area, indicating the EGCG displacement to hydrophobic zones (Figs. S5 and S6). Moreover, final RMSD levels of ECGC are compared to those observed for ATP. However, MD simulation of the EGCG interaction in the Arg-binding site showed stability only during the first ~40 ns with an RMSD of 0.5–0.8 nm (Fig. 6A). This behavior may be correlated to the first number of hydrogen bonds formed in Arg-binding site, compared to the hydrogen bonds observed at first steps in Arg-*Ll*AK interaction, and its reduction for the time of the simulation (Fig. S4).

Additionally, the MD trajectories generated were employed to perform an MM/PBSA analysis to calculate the binding free energy of ligand-*Ll*AK complexes during MD simulation and decomposition analysis. In the case of the Arg binding site, the binding free energy calculation of EGCG and arginine have compared energies of interaction during the first 30 ns. Still, simulation time >30 ns decreases the EGCG binding interaction (Fig. 6B). In addition, the free energy interaction is recovered at simulation time >60 ns, suggesting the displacement to another binding site. This behavior correlates to decomposition analysis, where EGCG interacts with other *Ll*AK residues (Thr^{273}, Tyr^{89}, and Val^{65}) but differs concerning arginine (Asp^{192}, Glu^{225}, and His^{315}) (Fig. 6C).

In this sense, we can observe that binding free energy calculated between EGCG and *Ll*AK in the ATP-binding site (Fig. 5B), is observed around −40 to −15 kcal/mol, confirming the stability of the EGCG interaction in this catalytic site. Likewise, low levels of binding free energies were observed with respect to ATP (−70 to −40 kcal/mol). Moreover, the decomposition analysis of the

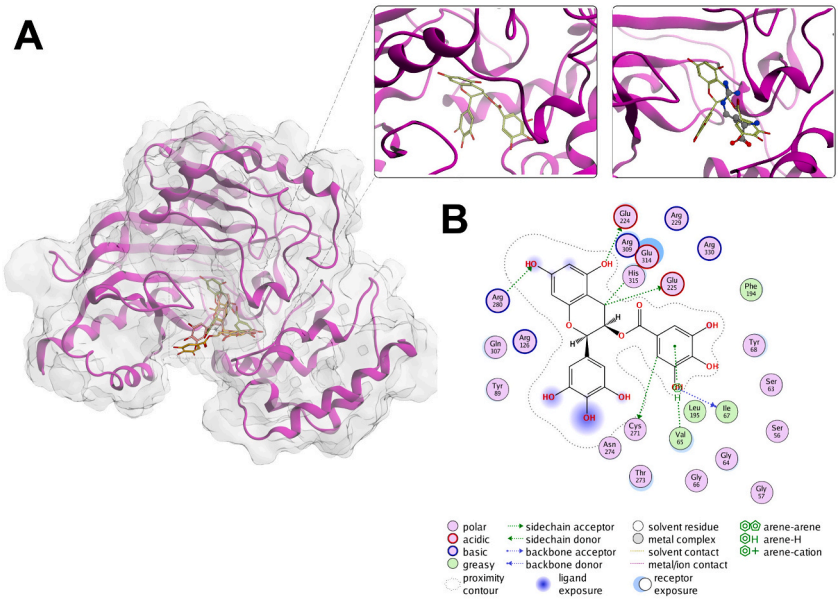

Fig. 4. Molecular docking of the interaction between *Ll*AK and EGCG at the arginine binding site. A) Surface map, ribbon representation of EGCG binding at the arginine pocket and superposition of arginine and EGCG structures. B) Lig-plot diagram of EGCG interactions at the arginine pocket. Color should be used for this figure in print.

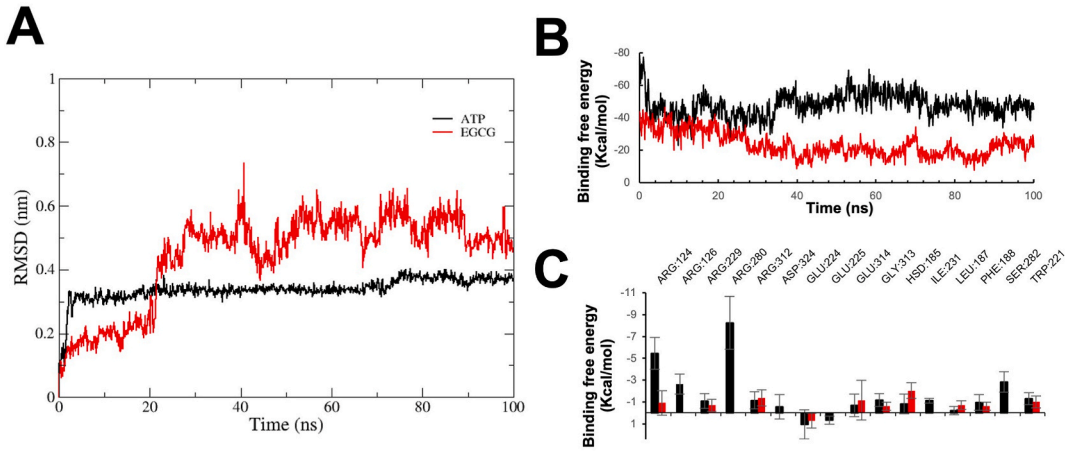

Fig. 5. Molecular dynamic and MMPBSA parameters in ATP binding site. A) EGCG to *Ll*AK Root mean square deviation (RMSD); B) Binding free energy of EGCG-*Ll*AK interaction; C) Decomposition analysis by *Ll*AK residue.

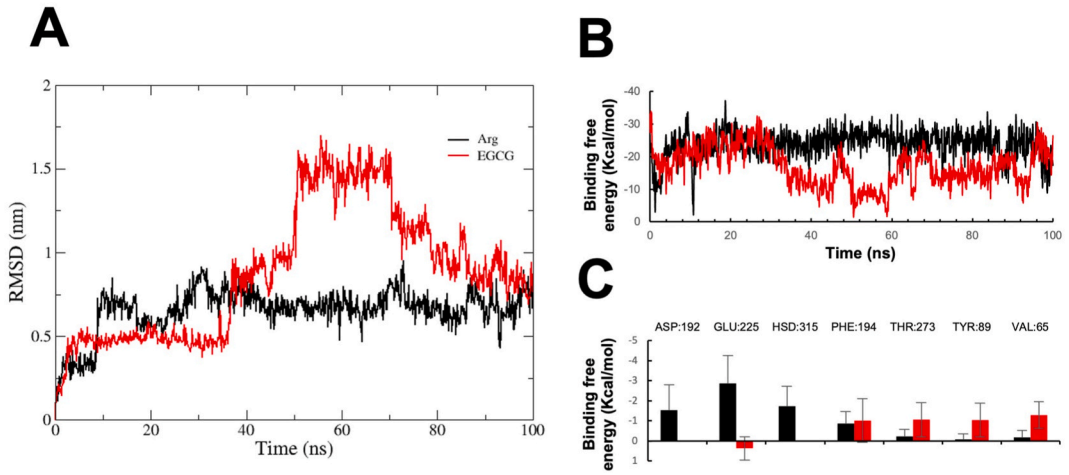

Fig. 6. Molecular dynamic and MMPBSA parameters in ARG binding site A) EGCG to *Ll*AK Root mean square deviation (RMSD); B) Binding free energy of EGCG-*Ll*AK interaction; C) Decomposition analysis by *Ll*AK residue.

trajectories of EGCG-*Ll*AK interaction in ATP-binding site reveals that the residues involved with more influence are Arg^{124}, Hsd^{185}, Trp^{221}, Arg^{229}, Ile^{231}, Arg^{312}, Gly^{313} and Glu^{314}, Phe^{188}, and Leu^{187} (Fig. 5C). However, it is noteworthy that among these residues, Arg^{312}, Hsd^{185}, Glu^{314} and Trp^{221} exhibited the most pronounced influence during the EGCG-*Ll*AK interaction.

3.5. *Interactions between LlAK and EGCG by fluorescence quenching*

Fluorescence emission spectra showed that *Ll*AK displayed a fluorescence emission maximum peak at 325 nm and its fluorescence was gradually quenched by increasing EGCG concentrations (Fig. 7A). EGCG showed a moderate binding affinity to *Ll*AK ($K_d = 58.3$ μM and $K_a = 1.71 \times 10^4$ M^{-1}) (Fig. 7B). To gain insight into the *Ll*AK-EGCG binding, Stern-Volmer plots were constructed. Fig. 8A shows a good linear relationship with the Stern-Volmer equation, with a K_{sv} value of 2.22×10^4 M^{-1}. The modified Stern-Volmer constant K_q was 1.63×10^4 M^{-1}, which agrees well with K_a and K_{sv} values. Furthermore, the fraction of fluorophore accessible to the quencher ($f_a = 1.05$) indicates that all Trp residues in *Ll*AK are accessible to EGCG. However, the results suggest that *Ll*AK has one binding site ($n = 1.03$) to EGCG (Fig. 8B and C; Table 2).

4. Discussion

AK plays an important role as a temporal energy buffering system during muscle contraction in invertebrates and links the phosphagen system with the glycolytic and mitochondrial respiration energy pathways to balance regeneration and ATP demand [19]. It is well-documented that the spider's muscular system contains few mitochondria, which provide the energy for their rapid

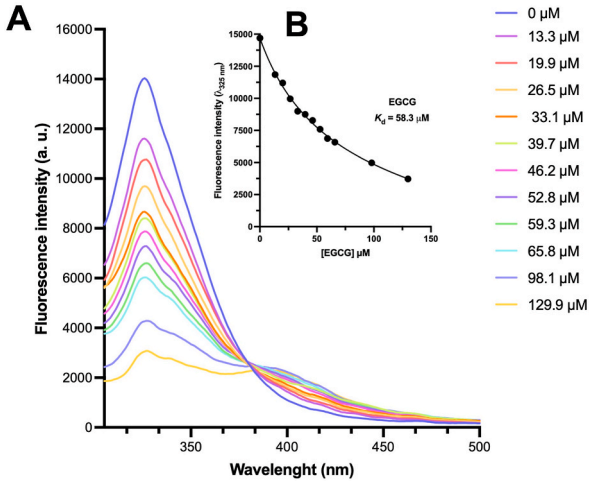

Fig. 7. Fluorescence emission spectra of *Ll*AK in the presence of EGCG. Inset: relationship between fluorescence emission maxima and EGCG concentration for K_d calculation by non-linear regression analysis.

movements to hunt or escape [60,61]. Spiders can achieve high levels of momentary activity; however, their muscles become exhausted after a few seconds of exertion, and thus, spiders use mainly anaerobic energy sources such as phosphate and glycogen [10, 61]. This feature suggests the significance of *Ll*AK participation in maintaining energy homeostasis in *L. laeta*, as the phosphagen system can sustain rapid movements when a quick energy burst is needed, and its kinetic characterization is necessary.

Our findings show that *Ll*AK shares sequence similarities with other spider AKs (such as *P. pythagoricus*, *L. tarantula,* and *L. hesperus*), but differs from creatine kinase as its counterpart in vertebrates. Furthermore, the *Ll*AK sequence revealed the presence of conserved arginine kinase domains and hallmarks of the phosphagen kinases superfamily, including the essential catalytic residues at the active site (Arg^{126}, Glu^{225}, Arg^{229}, Cys^{271}, Thr^{273}, Arg^{280}, Arg^{309} and Glu^{314}), the ATP/ADP and arginine binding sites, and the two specificity loops. Altogether, these conserved residues shape the AKs active site cleft between the small N-terminal and the large C-terminal domains, as reported in the crystal structures of *L. polyphemus*, *L. vannamei* and *P. pythagoricus* AKs [24,56,58]. Moreover, predicted *Ll*AK structures showed a phosphagen kinase fold. However, different conformations were observed between the open and closed structures, according to the AKs conformational changes to configure its active site and position the substrates in the proper geometry to perform catalysis [56,62–65].

Additionally, it is well known that specific activity among AKs is highly variable. In this sense, *Ll*AK had a reduced activity (1.1 U/mg) compared to AK activity of *L. vannamei* [41], *Dugestella hentzi* [42], and *Ctenocephalides felis* [66]. The variations in activity may be due to differences in the enzyme's physiological role and the metabolic and energetic demand of phosphagens in different organisms. Furthermore, the kinetic analysis demonstrated that *Ll*AK has a catalytic efficiency similar to the AK from *Rhipicephalus sanguineus* [54], which might be related to its important function in *L. laeta*'s bioenergetics and metabolism. This catalytic efficiency was reflected in L-arginine's low apparent K_m value, high turnover number (k_{cat}), and high k_{cat}/K_m ratio. Moreover, the sequence comparison analysis shows that the catalytic efficiency is not correlated to differences in active site residues, indicating an important role in the AKs structural conformation.

Thus, *Ll*AK is a toxicological target for the chemical control of *L. laeta* and, therefore, with significant medical implications due to its essential role in the bioenergetics of the spider. Developing innovative biopesticides can be achieved by identifying appropriate molecular targets unique to invertebrates and combining them with natural bioactive compounds (such as EGCG, the main polyphenol in green tea). This can provide a safer and more eco-friendly alternative to conventional pesticides because the flavonoids are biodegradable, and this property promotes low bioaccumulation [26,30,31]. In this regard, our results indicated that EGCG interacts preferentially at the ATP/ADP binding site from *Ll*AK, displaying higher free binding energies than those observed for ATP. Moreover, free binding energies of EGCG interactions at the arginine binding site were similar to the arginine substrate. This suggests that EGCG may bind to the *Ll*AK active site. Differential EGCG binding scores among ATP/ADP and arginine binding sites suggest a competitive inhibition mechanism for ADP/ATP or a non-competitive inhibition for arginine [65,67].

Recently, MD simulations have gained significant importance as a bioinformatic tool for assessing the interaction stability between polyphenol compounds and catalytic sites of biologically relevant enzymes. These simulations also help elucidate the underlying inhibitory mechanisms [68,69]. In the context of the present study, we have successfully confirmed that the stability of EGCG-*Ll*AK interaction is observed at the ATP/ADP-binding site throughout the simulation period, whose interaction can be influenced by hydrogen and hydrophobic bonds. It is noteworthy that the MM/PBSA analysis of the MD trajectories reveals a preference for EGCG to interact with key residues Hsd^{185}, Trp^{221}, Arg^{312}, and Glu^{314}, which play an important role in the catalytic activity of *Ll*AK. It is important to emphasize that Glu^{314} can be associated with the orientation of arginine for catalysis in the Arg-binding site and exhibits higher involvement during EGCG-*Ll*AK interaction [56,58]. This finding confirms the potential influence of EGCG preferentially at ATP/ADP catalytic site observed in molecular docking analysis and may contribute to *Ll*AK inhibition. As has been reported for other

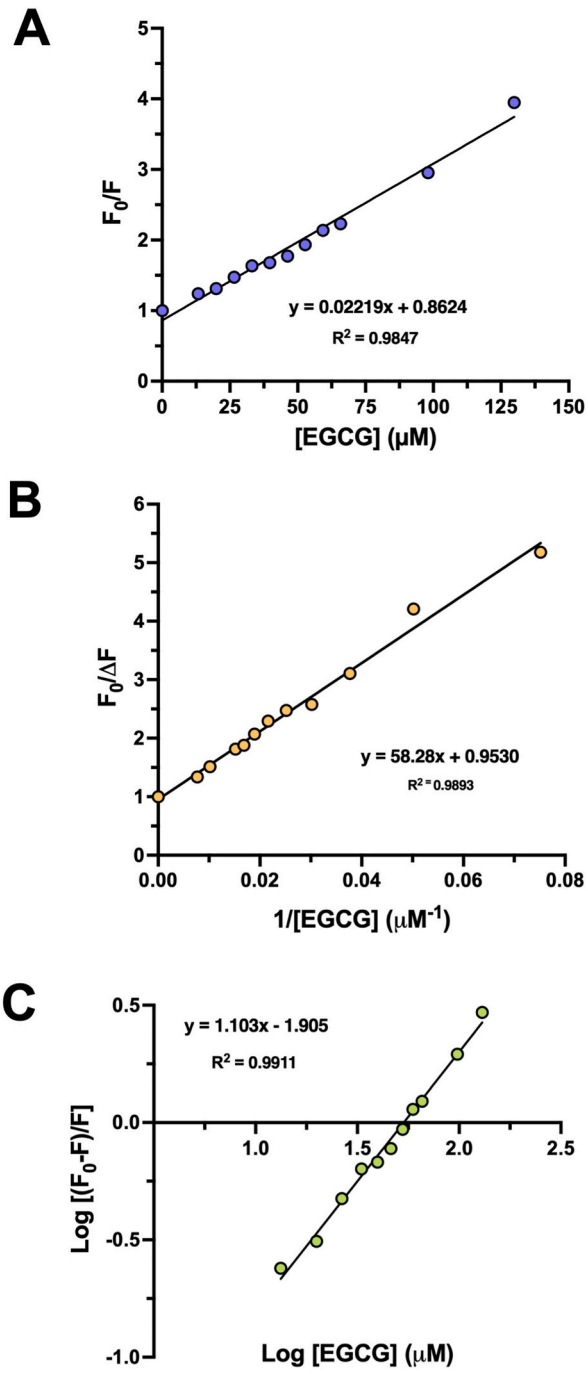

Fig. 8. Stern-Volmer plots of EGCG interaction with *Ll*AK. A) Stern-Volmer plot. B) Modified double reciprocal Stern-Volmer plot. C) Double logarithmic modified Stern-Volmer plot. Protein concentration was 1 μM and EGCG 0–130 μM.

phenolic compounds of varied molecular structures to inhibit the AK activity from insects and parasites [33–36,70].

Quenching of intrinsic tryptophan fluorescence is performed to investigate molecular interactions between proteins and ligands [52]. In this sense, *Ll*AK displayed a fluorescence emission characteristic (λ_{em}^{325nm}) for tryptophan residues partially buried, located in the non-polar environment [52], similarly reported to other AKs (such as *Stichopus japonicus*, *Locusta migratoria*, and *Trypanosoma brucei* [33,71,72]. Specifically, the findings obtained for fluorescence analysis of *Ll*AK-EGCG interaction showed a moderate binding affinity. Moreover, the λ_{em}^{325nm} of *Ll*AK had no shift concerning increments in the EGCG concentrations, suggesting that EGCG binding to *Ll*AK had no impact on the protein conformation.

Stern-Volmer analyses were conducted to gain insight into the *Ll*AK-EGCG binding process. Our results show that a homogeneous

Table 2
Binding parameters of *Ll*AK-EGCG complex.

	K_d (x10^{-6} M)[a]	K_a (x10^4 M^{-1})[a]	K_{sv} (x10^4 M^{-1})[b]	K_q (x10^4 M^{-1})[c]	f_a[c]	n[d]
EGCG	58.3	1.71	2.22 ± 0.0039	1.63 ± 8.55	1.05 ± 0.2778	1.103

[a] K_d values were calculated by non-linear regression analysis of the change in fluorescence intensities *versus* EGCG concentrations. K_a is the reciprocal of K_d.
[b] K_{sv} was calculated from the slope of Stern-Volmer plot (Eq. (2)).
[c] K_q and f_a values were calculated from the slope and y-intercept of the modifies Stern-Volmer plot (Eq. (3)), respectively.
[d] n was calculated from the slope of double-logarithmic plot (Eq. (4)).

population of emitting tryptophan fluorophores (all equally accessible to the quencher) or that only one mechanism of quenching (dynamic or static) is occurring during *Ll*AK-EGCG binding [48]. Moreover, the determined K_{sv} value indicates that *Ll*AK tryptophans and EGCG interact. In addition, all *Ll*AK tryptophane fractions are accessible to EGCG and there is one binding site of EGCG per *Ll*AK molecule ($n = 1.03$). This fluorescence behavior well-supported EGCG specificity to ATP/ADP binding site predicted by MD simulation because *Ll*AK contains a fully conserved Trp^{221} present in this binding site [71,73]. Furthermore, Trp^{221} participates in the free binding energy contribution of residues implicated in the interaction predicted by MM/PBSA analysis.

Loxoscelism is a public health problem caused by bites of *Loxosceles* spiders, which are commonly found in America. Identifying molecular targets in these spiders is important for developing new pest control strategies. AK plays a crucial role in the energetic metabolism of spiders and helps maintain their homeostasis. In this study, we described the *Ll*AK kinetic characteristics and analyzed the binding interactions between EGCG and *Ll*AK. This is the first report of an AK from a medically important spider species. The results of this research can provide valuable insights into developing new biopesticides that can reduce the negative impact of conventional pesticides, such as environmental contamination, health risks, and bioaccumulation. Even though the use of flavonoids is limited for its stability, this factor can be overcome using encapsulation and control release technologies [29,30,74]. In this sense, combining natural compounds with conventional pesticides can reduce pesticide use, providing a safer and eco-friendly alternative to manage dangerous *Loxosceles* species in urban areas.

Funding

We thank Consejo Nacional de Humanidades, Ciencias y Tecnologias (CONAHCYT) research grant CF-2019-610264, and for a postdoctoral scholarship to Dr. Elena N. Moreno-Cordova.

Data availability statement

Data from *Ll*AK enzyme kinetics and *Ll*AK-EGCG molecular interactions by fluorescence quenching and docking are available at repository “Raw data of *Ll*AK enzyme kinetics and molecular interactions between *Ll*AK and EGCG by docking, molecular dynamics and fluorescence quenching”, Mendeley Data, https://doi.org/10.17632/gjtxh3rv9s.1. The molecular dynamics trajectories from *Ll*AK-EGCG interactions are available from the corresponding authors upon request.

CRediT authorship contribution statement

Elena N. Moreno-Cordova: Writing – review & editing, Writing – original draft, Visualization, Validation, Resources, Methodology, Investigation, Formal analysis, Conceptualization. **Andres Alvarez-Armenta:** Writing – review & editing, Writing – original draft, Visualization, Validation, Software, Methodology, Investigation, Formal analysis. **Karina D. Garcia-Orozco:** Writing – review & editing, Validation, Supervision, Project administration, Methodology, Investigation, Data curation. **Aldo A. Arvizu-Flores:** Writing – review & editing, Visualization, Software, Investigation. **Maria A. Islas-Osuna:** Writing – review & editing, Supervision, Resources, Methodology, Investigation. **Ramon E. Robles-Zepeda:** Writing – review & editing, Supervision, Resources, Investigation, Funding acquisition. **Alonso A. Lopez-Zavala:** Writing – review & editing, Validation, Supervision, Resources, Methodology, Formal analysis. **Aldana Laino:** Writing – review & editing, Writing – original draft, Resources, Methodology, Investigation. **Rogerio R. Sotelo-Mundo:** Writing – review & editing, Writing – original draft, Supervision, Project administration, Investigation, Funding acquisition, Formal analysis, Conceptualization.

Declaration of competing interest

The authors declare the following financial interests/personal relationships which may be considered as potential competing interests:Rogerio R. Sotelo-Mundo, Ph.D. reports financial support, article publishing charges, equipment, drugs, or supplies, and statistical analysis were provided by Consejo Nacional de Humanidades, Ciencia y Tecnologia (Mexico). If there are other authors, they declare that they have no known competing financial interests or personal relationships that could have appeared to influence the work reported in this paper.

Appendix A. Supplementary data

Supplementary data to this article can be found online at https://doi.org/10.1016/j.heliyon.2024.e34036.

References

[1] R.S. Vetter, Spiders of the genus *Loxosceles* (Araneae, Sicariidae): a review of biological, medical and psychological aspects regarding envenomations, J. Arachnol. 36 (2008) 150–163. http://www.jstor.org/stable/25067882.

[2] G.K. Isbister, H.W. Fan, Spider bite, Lancet 378 (2011) 2039–2047, https://doi.org/10.1016/S0140-6736(10)62230-1.

[3] L.H. Gremski, D. Trevisan-Silva, V.P. Ferrer, F.H. Matsubara, G.O. Meissner, A.C.M. Wille, L. Vuitika, C. Dias-Lopes, A. Ullah, F.R. de Moraes, C. Chávez-Olórtegui, K.C. Barbaro, M.T. Murakami, R.K. Arni, A. Senff-Ribeiro, O.M. Chaim, S.S. Veiga, Recent advances in the understanding of brown spider venoms: from the biology of spiders to the molecular mechanisms of toxins, Toxicon 83 (2014) 91–120, https://doi.org/10.1016/j.toxicon.2014.02.023.

[4] G.J. Binford, M.S. Callahan, M.R. Bodner, M.R. Rynerson, P.B. Núñez, C.E. Ellison, R.P. Duncan, Phylogenetic relationships of *Loxosceles* and *Sicarius* spiders are consistent with Western Gondwanan vicariance, Mol. Phylogenet. Evol. 49 (2008) 538–553, https://doi.org/10.1016/j.ympev.2008.08.003.

[5] L.H. Gremski, H.C. da Justa, T.P. da Silva, N.L. Polli, B.C. Antunes, J.C. Minozzo, A.C. Wille, A. Senff-Ribeiro, R.K. Arni, S.S. Veiga, Forty years of the description of brown spider venom phospholipases-D, Toxins 12 (2020), https://doi.org/10.3390/toxins12030164.

[6] L.H. Gremski, H.C. da Justa, N.L. Polli, P.H. Schluga, J.L. Theodoro, A.C. Wille, A. Senff-Ribeiro, S.S. Veiga, Systemic loxoscelism, less frequent but more deadly: the involvement of phospholipases D in the pathophysiology of envenomation, Toxins 15 (2023), https://doi.org/10.3390/toxins15010017.

[7] P.H. da Silva, R.B. da Silveira, M. Helena Appel, O.C. Mangili, W. Gremski, S.S. Veiga, Brown spiders and loxoscelism, Toxicon 44 (2004) 693–709, https://doi.org/10.1016/j.toxicon.2004.07.012.

[8] A.L. de Souza, C.M. Malaque, J. Sztajnbok, C.C. Romano, A.J. Duarte, A.C. Seguro, *Loxosceles* venom-induced cytokine activation, hemolysis, and acute kidney injury, Toxicon 51 (2008) 151–156, https://doi.org/10.1016/j.toxicon.2007.08.011.

[9] J.K. Loden, D.L. Seger, H.A. Spiller, L. Wang, D.W. Byrne, Cutaneous-hemolytic loxoscelism following brown recluse spider envenomation: new understandings, Clin. Toxicol. 58 (2020) 1297–1305, https://doi.org/10.1080/15563650.2020.1739701.

[10] R. Solís, A. Alfaro, B. Segura, L. Moreno, M. Canals, Daily pattern of locomotor activity of the synanthropic spiders *Loxosceles laeta* and *Scytodes globula*, J. Arachnol. 46 (2018) 21–25, https://doi.org/10.1636/JoA-S-16-064.1.

[11] R.S. Vetter, G.K. Isbister, Medical aspects of spider bites, Annu. Rev. Entomol. 53 (2007) 409–429, https://doi.org/10.1146/annurev.ento.53.103106.093503.

[12] J. Rhoads, Epidemiology of the brown recluse spider bite, J. Am. Acad. Nurse Pract. 19 (2007) 79–85, https://doi.org/10.1111/j.1745-7599.2006.00201.x.

[13] N. Nguyen, M. Pandey, Loxoscelism: cutaneous and hematologic manifestations, Adv Hematol 2019 (2019) 4091278, https://doi.org/10.1155/2019/4091278.

[14] P.H. Lopes, C.C. Squaiella-Baptistão, M.O.T. Marques, D. V Tambourgi, Clinical aspects, diagnosis and management of *Loxosceles* spider envenomation: literature and case review, Arch. Toxicol. 94 (2020) 1461–1477, https://doi.org/10.1007/s00204-020-02719-0.

[15] A. Taucare-Ríos, W.H. Piel, Ecological niche divergence between the brown recluse spiders *Loxosceles laeta* and *L. surca* (Sicariidae) in Chile, J. Nat. Hist. 55 (2021) 1177–1193, https://doi.org/10.1080/00222933.2021.1937744.

[16] R.S. Vetter, S.A. Hedges, Integrated pest management of the brown recluse spider, J Integr Pest Manag 9 (2018) 4, https://doi.org/10.1093/jipm/pmx031.

[17] M.A. Navarro-Silva, J.E.L. Duque, E.N. Ramires, C.F.S. Andrade, E. Marques-Da-Silva, F.A. Marques, C.E. Delay, J.D. Fontana, A.C.S. Silva, G.M. Fraguas, Chemical control of *Loxosceles intermedia* (Araneae: sicariidae) with pyrethroids: field and laboratory evaluation, J. Econ. Entomol. 103 (2010) 166–171, https://doi.org/10.1603/EC09092.

[18] R. Ewing, H.N. Davis, B.L. Alstrom, C.E. Albin, A.M. Kragelund, R.J. Whitworth, Essential oils as an alternative to conventional pesticides for managing brown recluse spiders, *Loxosceles reclusa*, (Araneae: sicariidae), J. Kans. Entomol. Soc. 92 (2019) 406–411, https://doi.org/10.2317/0022-8567-92.1.406.

[19] W.R. Ellington, Evolution and physiological roles of phosphagen systems, Annu. Rev. Physiol. 63 (2001) 289–325, https://doi.org/10.1146/annurev.physiol.63.1.289.

[20] K. Uda, N. Fujimoto, Y. Akiyama, K. Mizuta, K. Tanaka, W.R. Ellington, T. Suzuki, Evolution of the arginine kinase gene family, Comp. Biochem. Physiol., Part D: Genomics Proteomics 1 (2006) 209–218, https://doi.org/10.1016/j.cbd.2005.10.007.

[21] H. Wang, L. Zhang, L. Zhang, Q. Lin, N. Liu, Arginine kinase: differentiation of gene expression and protein activity in the red imported fire ant, *Solenopsis invicta*, Gene 430 (2009) 38–43, https://doi.org/10.1016/j.gene.2008.10.021.

[22] A.C. Pereira, Arginine kinase: a potential pharmacological target in trypanosomiasis, Infect. Disord.: Drug Targets 14 (2014) 30–36, https://doi.org/10.2174/1871526514666140713144103.

[23] K.N. Prestwich, The constraints on maximal activity in spiders, J. Comp. Physiol. B 158 (1988) 437–447, https://doi.org/10.1007/BF00691141.

[24] A. Laino, A.A. Lopez-Zavala, K.D. Garcia-Orozco, J.S. Carrasco-Miranda, M. Santana, V. Stojanoff, R.R. Sotelo-Mundo, C.F. Garcia, Biochemical and structural characterization of a novel arginine kinase from the spider *Polybetes pythagoricus*, PeerJ 5 (2017) e3787, https://doi.org/10.2210/PDB5U92/PDB, e3787.

[25] N. Zhang, J. Wei, H. Jiang, H. Ge, Y. Zheng, X. Meng, K. Qian, J. Wang, Knockdown or inhibition of arginine kinases enhances susceptibility of *Tribolium castaneum* to deltamethrin, Pestic. Biochem. Physiol. 183 (2022) 105080, https://doi.org/10.1016/j.pestbp.2022.105080.

[26] M.S. Ayilara, B.S. Adeleke, S.A. Akinola, C.A. Fayose, U.T. Adeyemi, L.A. Gbadegesin, R.K. Omole, R.M. Johnson, Q.O. Uthman, O.O. Babalola, Biopesticides as a promising alternative to synthetic pesticides: a case for microbial pesticides, phytopesticides, and nanobiopesticides, Front. Microbiol. 14 (2023), https://doi.org/10.3389/fmicb.2023.1040901.

[27] Z. Zhao, M. Feng, J. Wan, X. Zheng, C. Teng, X. Xie, W. Pan, B. Hu, J. Huang, Z. Liu, J. Wu, S. Cai, Research progress of epigallocatechin-3-gallate (EGCG) on anti-pathogenic microbes and immune regulation activities, Food Funct. 12 (2021) 9607–9619, https://doi.org/10.1039/D1FO01352A.

[28] D. Mokra, M. Joskova, J. Mokry, Therapeutic effects of green tea polyphenol (−)-Epigallocatechin-3-gallate (EGCG) in relation to molecular pathways controlling inflammation, oxidative stress, and apoptosis, Int. J. Mol. Sci. 24 (2023), https://doi.org/10.3390/ijms24010340.

[29] V. Pereira, O. Figueira, P.C. Castilho, Flavonoids as insecticides in crop protection—a review of current research and future prospects, Plants 13 (2024), https://doi.org/10.3390/plants13060776.

[30] L. Schnarr, M.L. Segatto, O. Olsson, V.G. Zuin, K. Kümmerer, Flavonoids as biopesticides – systematic assessment of sources, structures, activities and environmental fate, Sci. Total Environ. 824 (2022) 153781, https://doi.org/10.1016/j.scitotenv.2022.153781.

[31] A. Khursheed, M.A. Rather, V. Jain, A.R. Wani, S. Rasool, R. Nazir, N.A. Malik, S.A. Majid, Plant based natural products as potential ecofriendly and safer biopesticides: a comprehensive overview of their advantages over conventional pesticides, limitations and regulatory aspects, Microb. Pathog. 173 (2022) 105854, https://doi.org/10.1016/j.micpath.2022.105854.

[32] C. Zhao, C. Ma, J. Luo, L. Niu, H. Hua, S. Zhang, J. Cui, Potential of cucurbitacin B and epigallocatechin gallate as biopesticides against *Aphis gossypii*, Insects 12 (2021), https://doi.org/10.3390/insects12010032.

[33] H.-R. Wang, W.-J. Zhu, X. Wang, Mechanism of inhibition of arginine kinase by flavonoids consistent with thermodynamics of docking simulation, Int. J. Biol. Macromol. 49 (2011) 985–991, https://doi.org/10.1016/j.ijbiomac.2011.08.017.

[34] X.-Q. Wu, W.-J. Zhu, Z.-R. Lü, Y. Xia, J.-M. Yang, F. Zou, X.-Y. Wang, The effect of rutin on arginine kinase: inhibition kinetics and thermodynamics merging with docking simulation, Int. J. Biol. Macromol. 44 (2009) 149–155, https://doi.org/10.1016/j.ijbiomac.2008.11.007.

[35] E. Valera-Vera, C. Reigada, M. Sayé, F.A. Digirolamo, F. Galceran, M.R. Miranda, C.A. Pereira, Trypanocidal activity of the anthocyanidin delphinidin, a non-competitive inhibitor of arginine kinase, Nat. Prod. Res. 36 (2022) 3153–3157, https://doi.org/10.1080/14786419.2021.1947270.

[36] E.A. Valera Vera, M. Sayé, C. Reigada, F.S. Damasceno, A.M. Silber, M.R. Miranda, C.A. Pereira, Resveratrol inhibits *Trypanosoma cruzi* arginine kinase and exerts a trypanocidal activity, Int. J. Biol. Macromol. 87 (2016) 498–503, https://doi.org/10.1016/j.ijbiomac.2016.03.014.

[37] M. Chauhan, V.K. Bhardwaj, A. Kumar, V. Kumar, P. Kumar, M.G. Enayathullah, J. Thomas, J. George, B.K. Kumar, R. Purohit, A. Kumar, S. Kumar, Theaflavin 3-gallate inhibits the main protease (Mpro) of SARS-CoV-2 and reduces its count *in vitro*, Sci. Rep. 12 (2022) 13146, https://doi.org/10.1038/s41598-022-17558-5.

[38] V.K. Bhardwaj, R. Singh, J. Sharma, V. Rajendran, R. Purohit, S. Kumar, Identification of bioactive molecules from tea plant as SARS-CoV-2 main protease inhibitors, J. Biomol. Struct. Dyn. 39 (2021) 3449–3458, https://doi.org/10.1080/07391102.2020.1766572.

[39] Y.-J. Li, F.-M. Gu, H.-C. Chen, Z.-X. Liu, W.-M. Song, F.-A. Wu, S. Sheng, J. Wang, Binding characteristics of pheromone-binding protein 1 in *Glyphodes pyloalis* to organophosphorus insecticides: insights from computational and experimental approaches, Int. J. Biol. Macromol. 260 (2024) 129339, https://doi.org/10.1016/j.ijbiomac.2024.129339.

[40] S.L. Blethen, Arginine kinase (arthropod muscle), Methods Enzymol. 17 (1970) 330–335. https://doi:10.1016/0076-6879(71)17206-0.

[41] K.D. García-Orozco, E. Aispuro-Hernández, G. Yepiz-Plascencia, A.M. Calderón-De-La-Barca, R.R. Sotelo-Mundo, Molecular characterization of arginine kinase, an allergen from the shrimp *Litopenaeus vannamei*, Int. Arch. Allergy Immunol. 144 (2007) 23–28, https://doi.org/10.1159/000102610.

[42] S.L. Blethen, N.O. Kaplan, Characteristics of arthropod arginine kinases, Biochemistry 7 (1968) 2123–2135, https://doi.org/10.1021/bi00846a015.

[43] M. de F. Fernandes-Pedrosa, I. de L.M. Junqueira-de-Azevedo, R.M. Gonçalves-de-Andrade, L.S. Kobashi, D.D. Almeida, P.L. Ho, D. V Tambourgi, Transcriptome analysis of *Loxosceles laeta* (Araneae, Sicariidae) spider venomous gland using expressed sequence tags, BMC Genom. 9 (2008) 279, https://doi.org/10.1186/1471-2164-9-279.

[44] E. Gasteiger, C. Hoogland, A. Gattiker, S. Duvaud, M.R. Wilkins, R.D. Appel, A. Bairoch, in: J.M. Walker (Ed.), Protein Identification and Analysis Tools on the ExPASy Server BT - the Proteomics Protocols Handbook, Humana Press, Totowa, NJ, 2005, pp. 571–607, https://doi.org/10.1385/1-59259-890-0:571.

[45] C. Notredame, D.G. Higgins, J. Heringa, T-coffee: a novel method for fast and accurate multiple sequence alignment, in: J. Thornton (Ed.), J. Mol. Biol. 302 (2000) 205–217, https://doi.org/10.1006/jmbi.2000.4042.

[46] F. Madeira, M. Pearce, A.R.N. Tivey, P. Basutkar, J. Lee, O. Edbali, N. Madhusoodanan, A. Kolesnikov, R. Lopez, Search and sequence analysis tools services from EMBL-EBI in 2022, Nucleic Acids Res. 50 (2022) W276–W279, https://doi.org/10.1093/nar/gkac240.

[47] S. Lu, J. Wang, F. Chitsaz, M.K. Derbyshire, R.C. Geer, N.R. Gonzales, M. Gwadz, D.I. Hurwitz, G.H. Marchler, J.S. Song, N. Thanki, R.A. Yamashita, M. Yang, D. Zhang, C. Zheng, C.J. Lanczycki, A. Marchler-Bauer, CDD/SPARCLE: the conserved domain database in 2020, Nucleic Acids Res. 48 (2020) D265–D268, https://doi.org/10.1093/nar/gkz991.

[48] F. Teufel, J.J. Almagro Armenteros, A.R. Johansen, M.H. Gíslason, S.I. Pihl, K.D. Tsirigos, O. Winther, S. Brunak, G. von Heijne, H. Nielsen, SignalP 6.0 predicts all five types of signal peptides using protein language models, Nat. Biotechnol. 40 (2022) 1023–1025, https://doi.org/10.1038/s41587-021-01156-3.

[49] M. Mirdita, K. Schütze, Y. Moriwaki, L. Heo, S. Ovchinnikov, M. Steinegger, ColabFold: making protein folding accessible to all, Nat. Methods 19 (2022) 679–682, https://doi.org/10.1038/s41592-022-01488-1.

[50] B. Gómez-Zaleta, G. Pérez-Hernández, H.I. Beltrán, F. Aparicio, A. Rojas-Hernández, A. Rojo-Domínguez, Molecular speciation effect on docking and drug design. A computational study for mangiferin, a carbohydrate-polyphenol bioconjugate as a test case, J Mex Chem Soc 52 (2008) 78–87.

[51] M.S. Valdés-Tresanco, M.E. Valdés-Tresanco, P.A. Valiente, E. Moreno, gmx_MMPBSA: a new tool to perform end-state free energy calculations with GROMACS, J Chem Theory Comput 17 (2021) 6281–6291, https://doi.org/10.1021/acs.jctc.1c00645.

[52] J. Lakowicz, Quenching of fluorescence, in: J.R. Lakowicz (Ed.), Principles of Fluorescence Spectroscopy, Springer US, Boston, MA, 2006, pp. 277–330, https://doi.org/10.1007/978-0-387-46312-4_8.

[53] S.S. Lehrer, Solute perturbation of protein fluorescence. Quenching of the tryptophyl fluorescence of model compounds and of lysozyme by iodide ion, Biochemistry 10 (1971) 3254–3263, https://doi.org/10.1021/bi00793a015.

[54] A.C. Gomez-Yanes, E.N. Moreno-Cordova, K.D. Garcia-Orozco, A. Laino, M.A. Islas-Osuna, A.A. Lopez-Zavala, J.G. Valenzuela, R.R. Sotelo-Mundo, The arginine kinase from the tick *Rhipicephalus sanguineus* is an efficient biocatalyst, Catalysts 12 (2022), https://doi.org/10.3390/catal12101178.

[55] S. Nitat, C. Wanpen, T. Anchalee, V. Pakit, B. Chaweewan, R. Pongrama, T. Pongsri, S. Yuwaporn, T. Pramuan, *Periplaneta americana* arginine kinase as a major cockroach allergen among Thai patients with major cockroach allergies, Environ. Health Perspect. 114 (2006) 875–880, https://doi.org/10.1289/ehp.8650.

[56] G. Zhou, T. Somasundaram, E. Blanc, G. Parthasarathy, R. Ellington W, M.S. Chapman, Transition state structure of arginine kinase: implications for catalysis of bimolecular reactions, Proc. Natl. Acad. Sci. USA 95 (1998) 8449–8454, https://doi.org/10.1073/pnas.95.15.8449.

[57] A. Azzi, The role of phosphagen specificity loops in arginine kinase, Protein Sci. 13 (2004) 575–585, https://doi.org/10.1110/ps.03428304.

[58] A.A. López-Zavala, K.D. García-Orozco, J.S. Carrasco-Miranda, R. Sugich-Miranda, E.F. Velázquez-Contreras, M.F. Criscitiello, L.G. Brieba, E. Rudiño-Piñera, R. R. Sotelo-Mundo, Crystal structure of shrimp arginine kinase in binary complex with arginine - a molecular view of the phosphagen precursor binding to the enzyme, J. Bioenerg. Biomembr. 45 (2013) 511–518, https://doi.org/10.1007/s10863-013-9521-0.

[59] K. Fritz-Wolf, T. Schnyder, T. Wallimann, W. Kabsch, Structure of mitochondrial creatine kinase, Nature 381 (1996) 341–345, https://doi.org/10.1038/381341a0.

[60] B. Linzen, P. Gallowitz, Enzyme activity patterns in muscles of the lycosid spider, *Cupiennius salei*, J. Comp. Physiol. 96 (1975) 101–109, https://doi.org/10.1007/BF00706589.

[61] R.F. Foelix, Biology of Spiders, third ed., Oxford University Press, Inc., New York, NY, 2011.

[62] M.S. Yousef, S.A. Clark, P.S. Pruett, T. Somasundaram, W.R. Ellington, M.S. Chapman, Induced fit in guanidino kinases–comparison of substrate-free and transition state analog structures of arginine kinase, Protein Sci. 12 (2003) 103–111, https://doi.org/10.1110/ps.0226303.

[63] O. Davulcu, Y. Peng, R. Brüschweiler, J.J. Skalicky, M.S. Chapman, Elevated μs-ms timescale backbone dynamics in the transition state analog form of arginine kinase, J. Struct. Biol. 200 (2017) 258–266, https://doi.org/10.1016/j.jsb.2017.05.002.

[64] S.A. Clark, O. Davulcu, M.S. Chapman, Crystal structures of arginine kinase in complex with ADP, nitrate, and various phosphagen analogs, Biochem. Biophys. Res. Commun. 427 (2012) 212–217, https://doi.org/10.1016/j.bbrc.2012.09.053.

[65] Y. Peng, A.L. Hansen, L. Bruschweiler-Li, O. Davulcu, J.J. Skalicky, M.S. Chapman, R. Brüschweiler, The Michaelis complex of arginine kinase samples the transition state at a frequency that matches the catalytic rate, J. Am. Chem. Soc. 139 (2017) 4846–4853, https://doi.org/10.1021/jacs.7b00236.

[66] M. Werr, J. Cramer, T. Ilg, Identification and characterization of two arginine kinases from the parasitic insect *Ctenocephalides felis*, Insect Biochem. Mol. Biol. 39 (2009) 634–645, https://doi.org/10.1016/j.ibmb.2009.07.001.

[67] Y. Blat, Non-competitive inhibition by active site binders, Chem. Biol. Drug Des. 75 (2010) 535–540, https://doi.org/10.1111/j.1747-0285.2010.00972.x.

[68] S.R. Sanjay Kottekad, U. Dandamudi, A computational study to probe the binding aspects of potent polyphenolic inhibitors of pancreatic lipase, J. Biomol. Struct. Dyn. (2023) 1–20, https://doi.org/10.1080/07391102.2023.2212795, 0.

[69] H. Liu, C. Zheng, Z. Li, X. Xia, D. Jiang, W. Wang, R. Zhang, X. Xiang, Inhibitory mechanism of phenolic compounds in rapeseed oil on α-amylase and α-glucosidase: spectroscopy, molecular docking, and molecular dynamic simulation, Spectrochim. Acta Mol. Biomol. Spectrosc. 289 (2023) 122251, https://doi.org/10.1016/j.saa.2022.122251.

[70] E.A. Valera-Vera, C. Reigada, M. Sayé, F.A. Digirolamo, F. Galceran, M.R. Miranda, C.A. Pereira, Effect of capsaicin on the protozoan parasite *Trypanosoma cruzi*, FEMS Microbiol. Lett. 367 (2020) fnaa194, https://doi.org/10.1093/femsle/fnaa194.

[71] Q. Guo, F. Zhao, S.-Y. Guo, X. Wang, The tryptophane residues of dimeric arginine kinase: roles of Trp-208 and Trp-218 in active site and conformation stability, Biochimie 86 (2004) 379–386, https://doi.org/10.1016/j.biochi.2004.05.006.

[72] O.S. Adeyemi, C.G. Whiteley, Interaction of nanoparticles with arginine kinase from *Trypanosoma brucei*: kinetic and mechanistic evaluation, Int. J. Biol. Macromol. 62 (2013) 450–456, https://doi.org/10.1016/j.ijbiomac.2013.09.008.

[73] M. Gross, E.M. Furter-Graves, T. Wallimann, H.M. Eppenberger, R. Furter, The tryptophan residues of mitochondrial creatine kinase: roles of Trp-223, Trp-206, and Trp-264 in active-site and quaternary structure formation, Protein Sci. 3 (1994) 1058–1068, https://doi.org/10.1002/pro.5560030708.

[74] E.V.R. Campos, P.L.F. Proença, J.L. Oliveira, M. Bakshi, P.C. Abhilash, L.F. Fraceto, Use of botanical insecticides for sustainable agriculture: future perspectives, Ecol Indic 105 (2019) 483–495, https://doi.org/10.1016/j.ecolind.2018.04.038.